Absence of Marangoni convection at Marangoni numbers above 27,000 during water evaporation

Ian Thompson,* Fei Duan,† and C. A. Ward‡
Thermodynamics and Kinetics Laboratory, Department of Mechanical and Industrial Engineering, University of Toronto, Toronto, Canada M5S 3G8

(Received 29 August 2008; revised manuscript received 15 August 2009; published 16 November 2009)

Two mechanisms by which Marangoni convection can be produced at the interface of water with its vapor are: (1) by imposing a temperature gradient parallel to the water-vapor interface, and (2) by imposing a temperature gradient perpendicular to the interface that results in the liquid becoming unstable. A series of evaporation experiments conducted with H_2O and with D_2O maintained at the mouth of a stainless-steel funnel indicated the presence of Marangoni convection, but the mechanism producing the convection was unclear. We have investigated the mechanism using a funnel constructed with a polymethyl methacrylate that has a small thermal conductivity relative to that of water and repeating the evaporation experiments. Marangoni convection was eliminated with this funnel even though the Marangoni number, Ma, was in the range $8277 \leq \mathrm{Ma} \leq 27\,847$. A comparison of the assumptions made in the theories available to predict the onset of Marangoni convection with the observations made in this study indicates some of the assumptions are invalid: although generally neglected, energy transport through the vapor to the interface of evaporating water is significant; there is an interfacial temperature discontinuity, but it is in the opposite direction of that assumed in the existing theories: the interfacial-vapor temperature is greater than that of the liquid during evaporation; and the prediction of the critical Marangoni number is based on an arbitrarily chosen value of the heat-transfer coefficient. When the temperature gradient is perpendicular to the water-vapor interface, these invalid assumptions indicate present theories do not apply to volatile liquids.

DOI: 10.1103/PhysRevE.80.056308 PACS number(s): 47.20.Dr, 47.55.dm

I. INTRODUCTION

An understanding of liquid stability during evaporation has proven important in numerous areas including particle deposition from evaporating droplets [1–7], in self-assembly [8–10], Czochralski crystal growth [11], and in energy transport at liquid-vapor interfaces [12–16]. Although water is a preferred solvent or energy-transport fluid in certain applications, the factors controlling its interfacial stability have been an open question for some time. One of the early reports of surface-tension-driven (or Marangoni) convection in water was that of Hershey [17], and his report was supported by that of Block [18]. These studies were only qualitative, and apparently resulted from imposing a temperature gradient *along* the liquid-vapor interface. There is little debate about the existence of Marangoni convection in water when a temperature gradient is imposed in this direction, but when the temperature gradient is imposed *perpendicular* to the interface, there is little agreement in the case of water. The transition from a quiescent interface to one with convection would then be initiated by a fluid instability, first discussed by Pearson [19].

He considered the stability of a liquid layer of finite depth and infinite extent, in the absence of gravity that was heated uniformly from below. He supposed that the gas above the liquid had a smaller temperature than did the interfacial liquid, and used the heat-transfer coefficient to define the cooling of the liquid. A linear perturbation analysis was performed to determine when a linear temperature profile in the liquid film would become unstable. If the Marangoni number (Table I) was greater than a critical value, $\mathrm{Ma}_{c\infty}$, that depended on the value of the heat-transfer coefficient, he predicted a transition from a quiescent film to one with surface-tension-driven convection. If the heat-transfer coefficient at the liquid-vapor interface were taken as zero, Pearson found that $\mathrm{Ma}_{c\infty}$ was 81. Nield [20] extended the Pearson model to take gravitational effects into account. He found the critical value of the Rayleigh number, Ra_{cr}, (see Table I) calculated in the absence of a surface-tension gradient to be 669, and that the critical value of the Marangoni number when gravity was acting, $\mathrm{Ma}_{cg\infty}$, could be calculated from

$$\frac{\mathrm{Ma}_{cg\infty}}{\mathrm{Ma}_{c\infty}} + \frac{\mathrm{Ra}}{\mathrm{Ra}_{cr}} = 1, \tag{1}$$

where Ra is the value of the Rayleigh number in the experiment. Note that according to this relation, if the liquid is stably stratified (the lighter liquid is above the heavier, $\mathrm{Ra} < 0$) buoyancy acts to stabilize the liquid against Marangoni convection, i.e., $\mathrm{Ma}_{cg\infty} > \mathrm{Ma}_{c\infty}$.

After the development of these basic theoretical models, a number of experimental investigations were conducted. The results can be put into two classes, according to the volatility of the liquid studied. Those studies using nonvolatile silcone oils obtained experimental results that supported the value of $\mathrm{Ma}_{cg\infty}$ predicted from the Pearson-Nield model [21,22], but the results found with volatile liquids have been controversial, particularly those obtained using water [23–26].

During water evaporation at conditions when $\mathrm{Ma} > \mathrm{Ma}_{cg\infty}$, Barnes and Feher [24] used interferometry to mea-

*Present address: IMP Aerospace, Enfield Nova Scotia B2T 1L5.
†Present address: Mechanical & Aerospace Engineering, Nanyang Technological University, Singapore 639798.
‡charles.ward@utoronto.ca

TABLE I. Parameters and dimensionless numbers.

ρ	Density	ν	Kinematic viscosity
η	Dynamic viscosity	α	Thermal diffusivity
κ	Thermal conductivity	κ_T	Coefficient of volume expansion
ϱ	Radial distance from centerline		
g	Gravity	h	Enthalpy
D	Diameter of the funnel mouth	c_p	Specific heat of the liquid.
c_σ	Surface-thermal capacity of the liquid	γ	Surface tension
$\gamma_T = \mathrm{d}\gamma/\mathrm{d}T$	Gradient of surface tension with temperature	j_{ev}	Evaporative mass flux
q	Heat flux	t	Time
v	Velocity	p	Pressure
T	Temperature	T_0	Throat temperature
$\Delta T = T_0 - T_I$	Temperature difference between the throat of the funnel and the interface	$\mathrm{Ra} = \kappa_T \Delta T g d^3/\nu\alpha$	Rayleigh number
$\mathrm{Ma} = \gamma_T \Delta T d/\rho\nu\alpha$	Marangoni number		
$\mathrm{Re} = vD/\nu$	Reynolds number	$\mathrm{Pr} = \nu/\alpha$	Prandtl number
$\Gamma = c_\sigma/\rho c_p d$	Nondimensional surface-thermal capacity number.		
Superscripts			
L	Liquid	V	Vapor
Subscript			
I	Interface		

sure the temperature as a function of depth, but their results did not indicate the presence of Marangoni convection. When others [25] found similar results, the existence of Marangoni convection in water that developed from an instability of the type defined by Pearson was questioned [26]. They could, as easily, have questioned the validity of the Pearson-Nield model when applied to water because that model does not strictly apply to volatile liquids (see below).

However, the Pearson-Nield model did receive *apparent* support from studies of H_2O and of D_2O evaporation from a stainless-steel funnel [13,14]. The funnel used in these studies is shown schematically in Fig. 1, and the observations are summarized in Table II. As seen there, provided the Marangoni number was greater than the value predicted to be critical by the Pearson-Nield model, Marangoni convection effects were observed in the energy transport [12–16]. They were also demonstrated by bringing the tip of a probe—a 12-μm-diameter cantilevered wire—in contact with both the H_2O and D_2O surfaces as each liquid evaporated steadily. The drag produced by the Marangoni flow around the cantilevered probe was shown to be sufficient to produce the observed probe deflection [12].

Clearly, the Pearson-Nield model indicates values of $\mathrm{Ma}_{cg\infty}$ that correlate with the measurements made with a stainless-steel funnel. However, this correlation must be viewed as surprising: firstly, because the measured interfacial-vapor temperature was greater than the interfacial-liquid temperature by several degrees, i.e., the temperature discontinuity was in the opposite direction to that assumed in the Pearson-Nield model. Secondly, since water is volatile, and was evaporating, the interface was the coldest place in the system. In general, there was energy transport to the interface from both the vapor and the liquid phases. In Figs. 2(A) and 2(B), the thermal conduction to the water-vapor

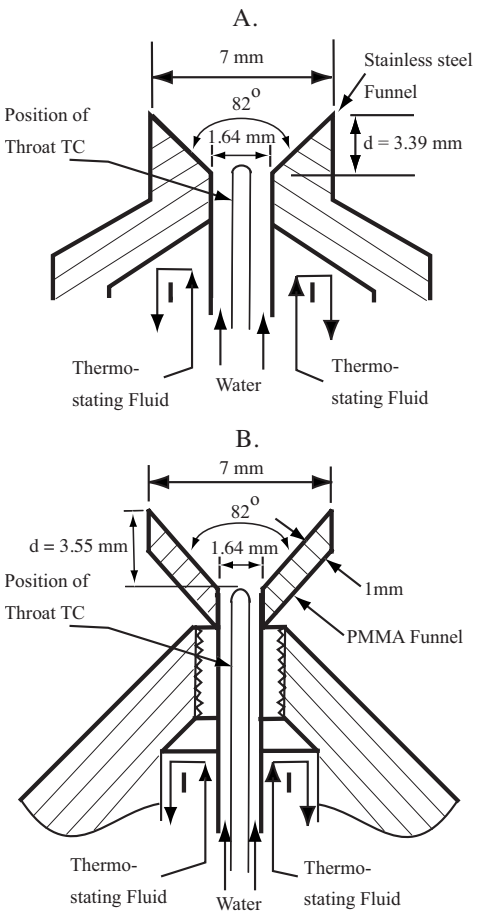

FIG. 1. The stainless-steel funnel used in the experiments of Duan and Ward [13,14] is shown in A, and the PMMA funnel for the work reported in this study is shown in B.

TABLE II. Conditions during steady-state H_2O and D_2O evaporation from a stainless-steel funnel [13,14].

Liquid, Expt:	H_2O, EV6	H_2O, EV7	H_2O, EV8	D_2O, EVD3	D_2O, EVD4	D_2O, EVD5
Vap.-ph. press. (Pa)	786.6	783.9	777.3	649.3	642.6	625.3
Avg. Evap. flux (mg/m^2 s)	63	70.0	100	81	89	221
Centr T_I^L (°C)	3.57	3.53	3.53	3.58	3.44	3.04
Ra_c	669	669	669	669	669	669
Ra	−0.27	−1.88	−7.07	−8.57	−121	−509
$Ma_{c\infty}$	81	81	81	81	81	81
$Ma_{cg\infty}$	81	81	81	82	96	143
Ma	10	127	447	69	298	1,267
Interface observed	Quiescent	Detectable conv.	Convection	Quiescent	Detectable conv.	Convection

interface from each phase in two experiments of the same series are shown [13]. In both cases, more energy was transferred through the vapor than through the liquid to the liquid-vapor interface. For the case indicated in Fig. 2(A), all of the energy to evaporate the liquid was transported through the vapor. Pearson and Nield assumed the vapor acted as an energy *sink*, but these results indicate that it acts more like an energy *source*. These considerations support the hypothesis that the Pearson model does not address the stability of a liquid if the liquid is evaporating.

This hypothesis is further supported by the changes in the conditions at the interface when the transition to surface-tension-driven convection occurred. When the evaporation rate was raised from 63 to 100 mg/m^2 s, Ma exceeded $Ma_{cg\infty}$, but a temperature gradient also developed along the interface, as indicated in Fig. 2(B). The temperature of the water at the funnel throat was maintained at ~3.5 °C in all experiments. Thus, there is the possibility that there was thermal conduction from the isothermal funnel throat through the stainless-steel walls to the colder circular mouth of the stainless-steel funnel, resulting in a temperature gradient being imposed from the funnel periphery to the center of the liquid-vapor interface. As indicated in Fig. 2, increasing the evaporation rate reduced the temperature at the interface compared to its value when the evaporation flux was 63 mg/m^2 s.

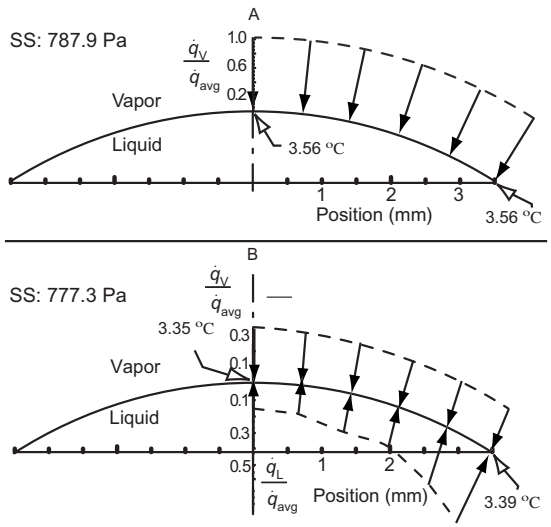

FIG. 2. The measured heat fluxes during two water-evaporation experiments are shown [13]. In A, the heat flux through the vapor and through the liquid are illustrated. Water was evaporating steadily at an average flux of 57 mg/m^2 s when the Marangoni number, Ma, was 5. Note there was no thermal conduction through the liquid. All of the energy to evaporate the liquid, 142.6 W/m^2, came through the vapor. In B, the average evaporation flux was raised to 100 mg/m^2 s, the average heat flux through the vapor was 132.58 W/m^2, that through the liquid was 117.28 W/m^2 and Ma was 447.

We examine this hypothesis by replacing the stainless-steel funnel with a polymethyl methacrylate (PMMA) one of similar geometrical design, and performing a series of evaporation experiments with it. The PMMA funnel is shown schematically in Fig. 1(B). The thermal conductivity of stainless steel is more than 26 times that of water, but PMMA is less than one-third that of water. Thus, the thermal conduction through the funnel walls from the throat to the funnel mouth was strongly reduced in these experiments. If heat conduction through the walls of the stainless-steel funnel were the source of the observed Marangoni convection, the PMMA funnel was expected to eliminate it.

II. EXPERIMENTAL PROCEDURE

The water used in the experiments was deionized (Barnstead Mega-Pure System), distilled, and nanofiltered (Barnstead D4751), resulting in water with a resistivity of 18.2 MΩ-cm and a surface tension that was within 1% of the documented value. After preparation, water was transferred into a glass flask and degassed. The temperature and vapor-phase pressure in the flask were measured at the end of the degassing process, and the pressure was found to agree with the documented value of the saturation-vapor pressure to within the measurement uncertainty.

From ″soak″ tests, the effect on the surface tension of water that resulted from water being pumped through the PMMA funnel was assessed and found to be negligible. A volume of 1.1 L of the prepared water without degassing was placed in each of two glass containers. Disks of PMMA with a total surface area of 92.2 cm^2 were added to one container. Both containers were closed and left in the lab for 28 days.

TABLE III. The experimental conditions on the center line during steady-state water evaporation from a PMMA funnel.

Experiment:	Expt 1	Expt 2	Expt 3	Expt 4	Expt 5
Vap.-ph. press. (Pa)	631	459	403	231	209
Max. intf. height (mm)	0.99	1.00	0.98	1.10	1.01
Intf. radius, R_0 (mm)	6.682	6.625	6.74	6.118	6.569
Avg. evap. flux (mg/m^2 s)	244	384	442	604	653
Centr. T_I^V (°C)	1.55	−2.52	−4.26	−10.25	−11.59
Centr. T_I^L (°C)	0.50	−3.92	−6.02	−13.11	−14.75
Throat temp. (°C)	3.58	3.53	3.57	3.47	3.50
Power req. (mW)	25.73 ± 0.13	40.16 ± 0.2	46.2 ± 0.2	64.9 ± 0.324	69.3 ± 0.35
Power sup. cond. (mW)	24.5 ± 2.16	39.995 ± 1.02	45.7 ± 0.89	64.7 ± 2.8	69.06 ± 1.0
Energy trans. liq. (%)	65.7	70	68.3	71	75.8
Re	0.0011	0.0015	0.0016	0.0016	0.0018
Ra	−717	−3,749	−5,881	−17,401	−19,362
$\mathrm{Ma}_{c\infty}$	81	81	81	81	81
$\mathrm{Ma}_{cg\infty}$	168	535	711	2,188	2,425
Ma	8,277	17,119	20,326	27,640	27,847
Interface observed	Quiescent	Quiescent	Quiescent	Quiescent	Quiescent

Eleven times during this period, 30 ml of water was taken from each container and the surface tensions and the temperature measured. The temperature was 25.85 ± 0.7 °C during this period. There was no statistical difference between the surface tensions of water and of the water exposed to PMMA. The measured surface tension of the (nondegassed) water was within 2% of the documented value at 25.85 °C.

In each experiment, degassed water was pumped directly, without exposure to air, from the degassing flask into the throat of the PMMA funnel that is shown schematically in Fig. 1(B). The funnel was enclosed in a chamber that allowed the vapor-phase pressure to be controlled. The water-vapor interface could be viewed from outside the chamber with a cathetometer. The water-pumping rate and the chamber pressure were adjusted so that during an experiment, the maximum height of the spherical water-vapor interface above the funnel mouth was approximately 1 mm and it did not move a detectable amount (± 10 μm) during an experiment. The water was pumped into the funnel throat with a syringe pump. Since the interface was unmoving, the water-evaporation rate was equal to the pumping rate which was accurately controlled (0.5% of the indicated value). The liquid-vapor interface contacted the funnel at the corner of the funnel mouth [see Fig. 1(B)] and was maintained at this position. A contact angle is not defined at this position.

The temperature of the water exiting the funnel throat was monitored with a thermocouple placed at that position and was maintained approximately constant at 3.5 °C with a circulating fluid. The actual values are listed in Table III. The evaporation cooled the water at the interface below that at the throat, and since water has its maximum density at 4 °C the lighter liquid was above the heavier. There was no buoyancy-driven convection during the experiments. The Rayleigh number was negative. According to the Nield model, the effect of buoyancy would have been to stabilize the liquid against Marangoni convection. As seen in Table III, the values of $\mathrm{Ma}_{cg\infty}$ are greater than $\mathrm{Ma}_{c\infty}$ because of the stabilizing effect of gravity when the fluid is stably stratified.

Once the evaporation was judged to have been occurring steadily for one hour, the temperature was measured with a microthermocouple (bead diameter <50 μm) that had been formed into a U shape, and placed on a positioning micrometer. The ratio of the horizontal wire length to the wire diameter was 60. In the axisymmetric system, the temperature was measured in cylindrical coordinates (ϱ, z) as a function of depth, z, and at five values of ϱ, on the funnel centerline and at horizontal positions 0.7, 1.4, 2.1, and 2.8 mm from the centerline. The funnel radius was 3.5 mm, but the thermocouple bead could not be placed in the liqiud phase closer than 0.7 mm of the funnel periphery. At one value of ϱ, when the temperature closest to the interface was measured in the liquid and vapor phases, the position of the center of the thermocouple bead was approximately 30 μm below or above the interface. We take these temperatures to be equal to the interfacial temperatures in the vapor and liquid phases at that value of ϱ. Once the thermocouple had been placed at a particular position, the temperature was recorded each second for a period of 30 s with a data-acquisition system, and its mean value and standard deviation determined.

The Reynolds number of the flow was of order 10^{-3}. The symmetry of the temperature field was examined by turning the positioning micrometer 90°, and measuring a second radial profile. As might be expected for the creeping flow of these experiments, the temperature field was symmetric to within the measurement error in both the liquid and vapor phases.

III. EXPERIMENTAL RESULTS

The conditions in each of the experiments are summarized in Table III. The interfacial temperatures in the liquid and

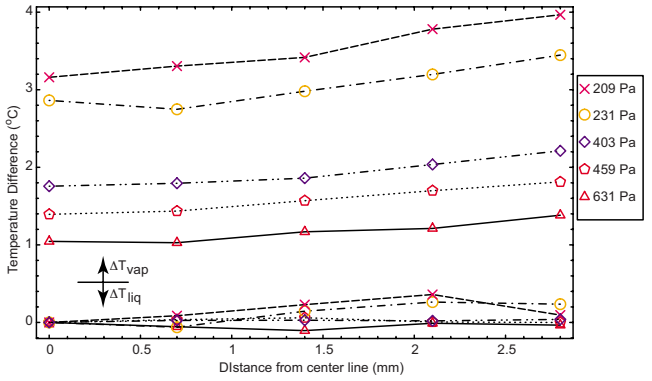

FIG. 3. (Color online) For five experiments, the difference between the centerline-interfacial-liquid temperature and the interfacial-liquid temperature at four positions along the interface are shown by the five lower curves. Also, the interfacial-vapor temperature relative to the center line-interfacial-liquid temperature are shown by the upper five curves.

vapor phases measured at five positions along the interface are shown in Fig. 3 for each experiment. The temperature values shown are relative to the interfacial-liquid temperature on the center line. If the temperature in the liquid phase is denoted T_I^L and position on the spherical liquid-vapor interface as (R_0,θ), then there was no clear trend in the interfacial-liquid temperature, i.e., $T_I^L(R_0,\theta)$, was approximately constant. Thus, the PMMA funnel eliminated the interfacial-liquid-temperature profile that had been observed with the stainless-steel funnel. This suggests it also eliminated the Marangoni convection, since there was then no gradient in surface tension along the interface. We investigate this possibility further in two ways.

A. Conservation of energy

We assume there was no energy transport by Marangoni convection and determine if the conservation-of-energy principle is satisfied. It was previously found that if Marangoni convection were present, the conservation-of-energy principle could not be satisfied without taking energy transport by Marangoni convection into account [13,14,16].

If the interface is quiescent, then in spherical coordinates (r,θ) conservation of energy requires

$$\kappa^V\left(\frac{\partial T^V}{\partial r}\right)_{\theta,I} - \kappa^L\left(\frac{\partial T}{\partial r}\right)_{\theta,I} = j_{ev}[h^V(T_I^V) - h^L(T_I^L)], \qquad (2)$$

where T^V denotes the temperature in the vapor and the subscript I on a quantity indicates it is to be evaluated at the interface (i.e., at $r=R_0$). The local evaporation flux is denoted j_{ev}, the enthalpies, the thermal conductivities in the liquid and vapor phases are denoted h^V, h^L, κ^V, and κ^L, respectively.

The temperature in each phase is assumed to be axisymmetric. In each experiment, it was measured in cylindrical coordinates (ϱ,z) as a function of z at each of the five ϱ values (0, 0.7, 1.4, 2.1, and 2.8 mm). The results obtained in experiment 4 are shown in Fig. 4.

The temperature gradient in spherical coordinates may be expressed as

$$\left(\frac{\partial T}{\partial r}\right)_\theta = \frac{\tan\theta}{r}\left(\frac{\partial T}{\partial \theta}\right)_r + \left(\frac{\partial T}{\partial z}\right)_\varrho \frac{1}{\cos\theta}. \qquad (3)$$

At the interface $(r=R_0)$, since $T^L(R_0,\theta)$ was constant for the different values of θ, the first term in Eq. (3) vanishes,

$$\left(\frac{\partial T^L}{\partial r}\right)_{\theta,I} = \left(\frac{\partial T^L}{\partial z}\right)_{\varrho,I} \frac{1}{\cos\theta_I}. \qquad (4)$$

The results in Fig. 4 indicate that at a value of ϱ_i, $T^L(\varrho_i,z)$ may be expressed as a first-order polynomial in z and the coefficients determined from linear regression. Then heat flux from the liquid to the interface may be calculated from Eq. (4).

In the vapor, as indicated in Fig. 3, $(\partial T^V/\partial\theta)$ does not vanish so both terms in Eq. (3) were used to evaluate the temperature gradient in spherical coordinates. The

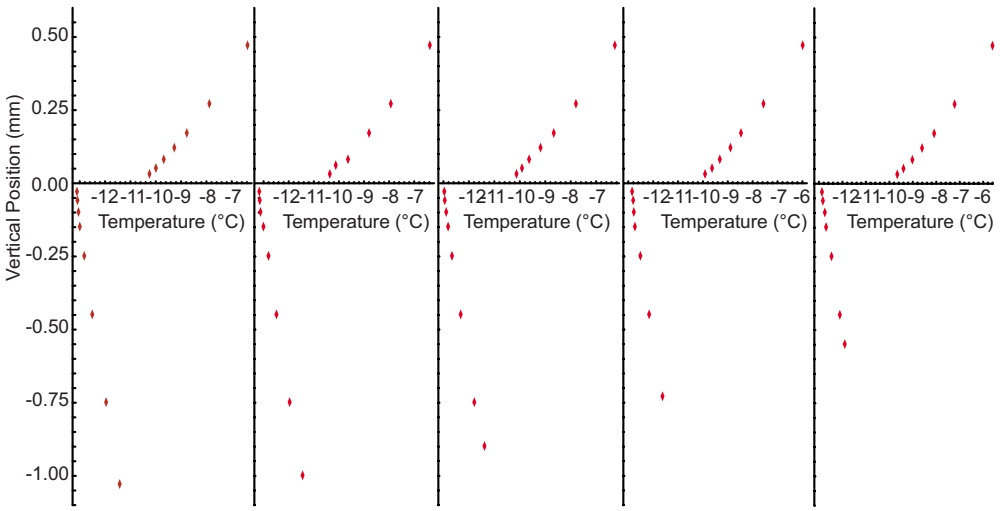

FIG. 4. (Color online) The temperature measured in Expt 4 (see Table III) as a function of z at five horizontal positions: 0, 0.7, 1.4, 2.1, and 2.8 mm.

interfacial-vapor temperature in spherical coordinates, $T(R_0,\theta)$ was assumed to be a second-order polynomial in $\cos\theta$,

$$T_I^V(R_0,\theta) = a_0 + a_1 \cos\theta + a_2 \cos^2\theta. \quad (5)$$

The coefficients were evaluated by linear regression using the measured interfacial-vapor temperatures. The same numerical procedure was used in the vapor as used in the liquid to evaluate the second term in Eq. (3), except a third order polynomial was used to determine $T^V(\varrho_i,z)$. This allowed the heat flux from the vapor to the interface to be determined. The power supplied to the interface by heating, $\dot{Q}_c$, is given by

$$\dot{Q}_c = 2\pi \int_0^{\theta_{max}} [-\kappa^L(\partial T^L/\partial r)_{\theta,I} + \kappa^V(\partial T^V/\partial r)_{\theta,I}] R_0^2 \sin\theta d\theta, \quad (6)$$

where θ_{max} is the polar angle at which the liquid-vapor interface meets the periphery of the funnel, and is equal to $\arcsin(x_m/R_0)$, where x_m is the radius of the funnel mouth, 3.5 mm.

The power required to evaporate the liquid at the observed rate, $\dot{E}_r$, can be obtained independently of the measured temperature profiles, and is given by

$$\dot{E}_r = 2\pi \int_0^{\theta_{max}} [j_{ev}(h^V - h^L)] R_0^2 \sin\theta] d\theta. \quad (7)$$

The enthalpy difference can be determined from

$$h^V(T_I^V) - h^L(T_I^L) = h_{fg}(T_{3p}) + c_p^V(T_I^V - T_{3p}) - c_p^L(T_I^L - T_{3p}), \quad (8)$$

where T_{3p} is the triple-point temperature, and c_p is the constant-pressure specific heat. The enthalpy difference was calculated at each of the five measurement locations and found to vary by less than 0.1%. Thus, the average value is used in the calculations. The constant evaporation rate, J_{ev}, is taken to be the syringe pump reading. The power required to evaporate the liquid at the measured rate is then

$$\dot{E}_r = J_{ev}(h_I^V - h_I^L)_{avg}. \quad (9)$$

In each phase, the error in the values of $\dot{Q}_c$ was assumed to result from the error in the fitting procedures, the error in the calibration of the thermocouples ($\sim$0.03 °C), and the error in the measurement of the z positions of the thermocouple (± 10 μm). These errors were then combined [27] to give the vertical error bars seen in Fig. 5. The horizontal error bars resulted from the error in $(h_I^V - h_I^L)$ and the error in the syringe pumping rate. They are not visible in Fig. 5. The vertical error bars are large because of the necessity of extrapolating the third order polynomial to the funnel periphery. As seen in this figure, in each experiment the power supplied to the interface by thermal conduction was sufficient to evaporate the liquid at the observed rate.

Two methods for detecting Marangoni convection have been previously examined. In one a flow probe was used [12]. As water evaporated steadily while at the mouth of the stainless-steel funnel [Fig. 1(A)] the tip of a cantilevered-12.5 μm-diameter wire was inserted 40 μm into the evaporating liquid. If the flow parallel to the interface was of sufficient magnitude, the stiffness of the probe could be overcome and the probe deflected. It was found that when the flow speed was greater than 0.63 ± 0.02 mm/s (corresponding to a vapor-phase pressure of 600 Pa) the probe deflection could be measured.

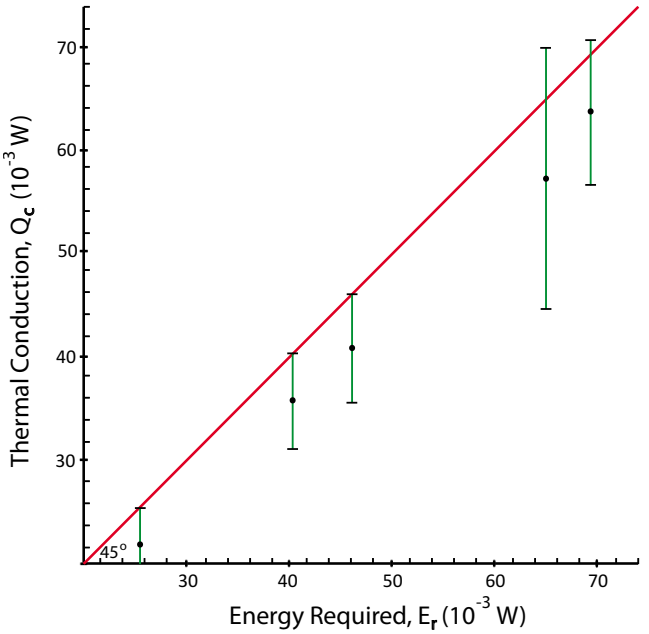

FIG. 5. (Color online) Comparison of power supplied to the liquid-vapor interface by thermal conduction, $\dot{Q}_c$, with the power required to evaporate the liquid at the observed rate, $\dot{E}_r$.

In the second, more sensitive method for detecting Marangoni convection, an investigation of the energy transported by Marangoni convection was examined. Energy transported by this mechanism depends on the surface-thermal capacity of the liquid [13]. In the circumstance considered, the liquid was stably stratified, and radiation was negligible; thus, the only active energy-transport mechanisms were thermal conduction and possibly Marangoni convection. So long as the measured temperature profiles in the liquid and vapor phases indicated thermal conduction supplied the energy required to evaporate the liquid, no Marangoni convection could be detected.

As the evaporation flux was increased further, by lowering the pressure in the vapor phase, a condition was reached where the conservation-of-energy principle could no longer be satisfied without taking energy transport by Marangoni convection into account. Two changes in the temperature field were then observed:

(1) a temperature gradient along the interface developed, $\nabla T_I^L \cdot i_\theta$, that was measurable where none had been discernible before;

(2) a uniform-temperature layer, of thickness δ_u, developed in the liquid immediately below the interface was then measurable. An expression for the speed parallel to the liquid-vapor interface, $v_\theta(R_0,\theta)$, was obtained from the Marangoni stress condition [12],

$$v_\theta(R_0,\theta) = -\frac{1}{\eta}\left(\frac{d\gamma^{LV}}{dT_I^L}\right)(\nabla T_I^L \cdot i_\theta)\ln\left(1-\frac{\delta_u}{R_0}\right) \qquad (10)$$

where R_0 is the radius of the spherical interface, and η is the viscosity. In the experiments of reference [13], this second method could detect Marangoni speeds as low as 0.22 mm/s which corresponds to an energy transport of 0.6 mW, and a δ_u value of 0.080 mm. Thus, this method for detecting Marangoni convection is much more sensitive than the probe.

The measurements made in this study indicate the Marangoni speed is zero for three reasons:

(1) as seen in Fig. 3, there was no measurable temperature gradient along the interface; thus, $\nabla T_I^L \cdot i_\theta = 0$, and Eq. (10) then indicates v_θ is zero;

(2) the measured temperature profiles as a function of depth for experiment 4 (see Table III) are shown in Fig. 4. As seen there, no uniform-temperature layer is discernible at any position along the interface. Similar results were found with the other experiments. Thus, δ_u was zero in each case, and Eq. (10) indicates $v_\theta(R_0,\theta)$ is then also zero.

(3) These results appear to be confirmed by the results shown in Fig. 5. As seen there, although an extrapolation in the temperature profile was necessary, thermal conduction appears to supply the energy required to evaporate the liquid at the measured rate. In reference [13] it was found that when this condition was met, Marangoni convection could not be detected. The error bars on the thermal conduction in these experiments are larger than on the experiments of reference [13], perhaps because the interfacial-liquid temperatures were so much lower in this case than in the earlier experiments, as may be seen by comparing the centerline-interfacial-liquid temperatures listed in Tables II and III. The lowest temperatures in the two cases were 3.53 and −14.57 °C. This made the thermal conditions much harder to control in these experiments. Because of the error bars, energy transport by Marangoni convection of as much as ±1 mW would have been within the error bars. However, if Marangoni convection were present, there is no reason we would not have been able to measure a temperature gradient along the interface or a uniform-temperature layer. Thus, not the measured temperature parallel to the interface, nor the measured temperature as a function of depth nor the comparison of thermal conduction with the power required to evaporate water at the measured rate indicates the presence of Marangoni convection.

B. Prediction of the saturation-vapor pressure when Marangoni convection is assumed absent

To further assess for the possible presence of Marangoni convection, we assume there was no Marangoni convection in any of the experiments, and use the data with statistical rate theory (SRT) [28–33] and predict the value of the saturation-vapor pressure, $P_s(T)$, at each position on the interface where measurements were made. The predicted values of the saturation-vapor pressure can then be compared with the values calculated from an expression for the saturation-vapor pressure that has been previously proposed and experimentally examined [32]. The expression for $P_s(T)$ has been shown to allow predictions of the latent heat and the constant-pressure specific heat that are in agreement with independent measurements of these properties.

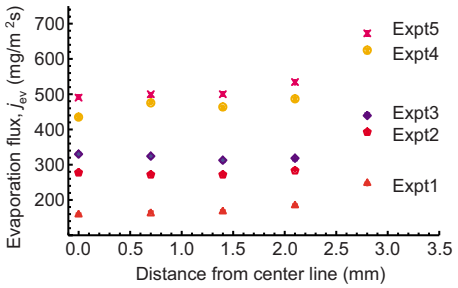

FIG. 6. (Color online) The local evaporation flux as a function of position from the centerline.

Statistical rate theory leads to an expression for the evaporation flux, j_{ev}, in terms of the interfacial temperatures and pressures in each phase and contains P_s as a parameter to be evaluated at the interfacial-liquid temperature [30–35]. In each experiment, T_I^L did not change measurably along the interface, but had different values in the different experiments. (See Table III and Fig. 3.) Thus, in each experiment, the same value of $P_s(T_I^L)$ at points along the interface should be obtained from the measurements made.

If there is no Marangoni convection, the local evaporation flux can be determined from Eq. (2) and the measured temperature profiles. One finds the results shown in Fig. 7.

From SRT, the expression for the evaporation flux is

$$j_{ev} = 2K_e \sinh\left(\frac{\Delta s_{LV}}{k_b}\right), \qquad (11)$$

where k_b is the Boltzmann constant. If the specific volume at saturation of the liquid phase is denoted v_f, and that of the vapor as v_g, and m_w denotes the molecular mass, then K_e is given by

$$K_e = \frac{P_s(T_I^L)\exp[(v_f/v_g)(P^L/P_s(T_I^L)-1)]}{\sqrt{2\pi m_w k_b T_I^L}} \qquad (12)$$

and Δs_{LV} is the entropy change that results from a molecule transferring from the liquid to the vapor and may be expressed [30]:

$$\frac{\Delta s_{LV}}{k_b} = 4\left(1-\frac{T_I^V}{T_I^L}\right) + \left(\frac{1}{T_I^V}-\frac{1}{T_I^L}\right)\sum_{l=1}^{3}\left(\frac{\hbar\omega_l}{2k_b} + \frac{\hbar\omega_l}{k_b[\exp(\hbar\omega_l/k_bT_I^V)-1]}\right) + \frac{v_f}{k_bT_I^L}[P_I^V + \gamma^{LV}(R_1^{-1} + R_2^{-1}) - P_s(T_I^L)] + \ln\left[\left(\frac{T_I^V}{T_I^L}\right)^4\left(\frac{P_s(T_I^L)}{P_I^V}\right)\right] + \ln\left(\frac{q_{vib}(T_I^V)}{q_{vib}(T_I^L)}\right), \qquad (13)$$

where γ^{LV} is the surface tension, R_1 and R_2 are the interface radii, and the vibration partition function is given by

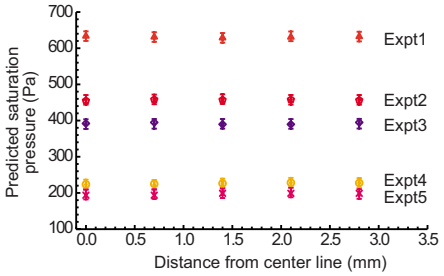

FIG. 7. (Color online) The local evaporation flux as a function of position from the center line.

$$q_{vib}(T) \equiv \prod_{l=1}^{3} \frac{\exp(-\hbar\omega_l/2k_bT)}{1-\exp(-\hbar\omega_l/k_bT)}, \tag{14}$$

where ω_l denotes the fundamental frequencies of the covalent bonds of the water molecule. The molecular vibration modes are symmetric stretch (3651 cm^{-1}), asymmetric stretch (3756 cm^{-1}) and bending (1590 cm^{-1}) [36].

The values of γ^{LV} and v_f are given in [37,38], respectively,

$$\gamma^{LV} = 10^{-3}[75.478\ 70 - 0.138\ 48(T-273.15) - 3.363\ 92 \times 10^{-4}(T-273.15)^2 + 4.753\ 62 \times 10^{-7}(T-273.15)^3 + 2.644\ 79 \times 10^{-10}(T-273.15)^4], \tag{15}$$

$$v_f = 10^{-3}(334.601\ 163 - 6.962\ 367T + 6.067\ 943 \times 10^{-2}T^2 - 2.825\ 583 \times 10^{-4}T^3 + 7.411\ 762 \times 10^{-7}T^4 - 1.038\ 083 \times 10^{-9}T^5 + 6.063\ 848\ 4 \times 10^{-13}T^6). \tag{16}$$

In the experiments we consider, the maximum height of the liquid-vapor interface above the funnel mouth was approximately 1 mm (see Table III). In this circumstance, the interface may be approximated as spherical,

$$R_1 = R_2 \equiv R_0,$$

and if its maximum height is denoted z_0 and the funnel-mouth radius as x_m, then

$$R_0 = \frac{x_m^2 + z_0^2}{2z_0}. \tag{17}$$

From the Laplace equation

$$P^L = P^V + \frac{2\gamma^{LV}}{R_0}. \tag{18}$$

When Eqs. (12)–(16) and (18) are combined with Eq. (11), one obtains an expression for the evaporation flux that is in terms of the instantaneous interfacial properties T_I^L, T_I^V, P_I^V, R_0, and the material properties of water: $P_s(T_I^L)$, v_f, γ^{LV}, and the internal vibration frequencies of the water molecule, ω_l. Since there are no free or fitting parameters in the SRT equations for the evaporation flux, the value of $P_s(T_I^L)$ is the only unknown in the system of equations, and its value may then be determined numerically.

The values obtained are those shown in Fig. 7. In each experiment, since there was no variation in the temperature, no variation in the calculated values of P_s along the interface was expected. However, the interface liquid temperature had different values in the different experiments. This allows the value $P_s(T_I^L)$ as a function of temperature to be determined. The values obtained in the different experiments are shown in Fig. 8.

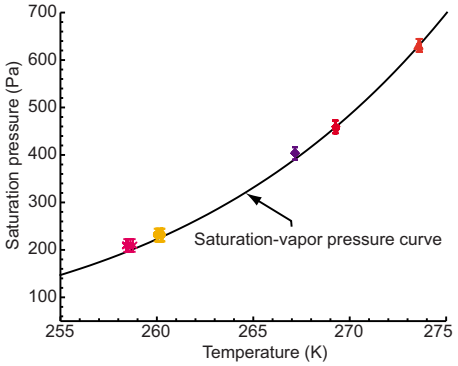

FIG. 8. (Color online) Calculated values of the saturation-vapor pressure from the measurements and statistical rate theory (data point) and P_s calculated using Eq. (19).

The numerical values of P_s obtained from the measurements can be assessed by comparing them with those calculated from an expression recently proposed for $P_s(T)$ [32],

$$P_s = 611.2 \exp[1045.851\ 157\ 7 - 21\ 394.666\ 262\ 9/T + 1.096\ 904\ 4T - 1.300\ 374\ 1 \times 10^{-3}T^2 + 7.747\ 298\ 4 \times 10^{-7}T^3 - 2.164\ 900\ 5 \times 10^{-12}T^4 - 211.389\ 655\ 9 \ln(T)]. \tag{19}$$

In Fig. 8, the values of P_s calculated from Eq. (19) are shown as a solid line. The values of P_s obtained along the interface from each experiment, Fig. 7, have been averaged and their standard deviations calculated. They are shown as data points with the standard deviations as the error bars in Fig. 8. As seen there, under the assumption of no Marangoni convection, no measured difference was found between the values of P_s determined from the experiments with the PMMA funnel, and the values of P_s determined from Eq. (19).

We note that if the same procedure were used to examine the experiments conducted with the stainless-steel funnel, the deviation between the values of P_s calculated from Eq. (19) is greater than 10% at 262 K [39]. Thus, the agreement seen in Fig. 8 supports the hypothesis that there was no Marangoni convection in the water-evaporation experiments when the evaporation took place at the mouth of the PMMA funnel.

IV. DISCUSSION AND CONCLUSION

Two mechanisms of producing Marangoni convection in water are commonly discussed: one is by imposing a temperature gradient parallel to the interface of water with its vapor, and the other is that hypothesized to result from a fluid instability that occurs when the Marangoni number exceeds a limiting value. In the experiments of this study, even

though the Marangoni number was $8\,277 \leq \mathrm{Ma} \leq 27\,847$, no Marangoni convection was detected from an examination of four independent parameters:

(1) there was no measurable temperature gradient along the interface;

(2) no uniform-temperature layer in the liquid immediately below the interface could be detected, whereas one was present when Marangoni convection was present in earlier experiments;

(3) although an extrapolation of the temperature to the periphery (from 2.8 to 3.5 mm) was necessary, the indication is that thermal conduction supplied the power required to evaporate the liquid at the measured rate;

(4) when Marangoni convection was assumed absent and the evaporation flux along the interface was used with SRT to predict $P_s(T_I^L)$, the values obtained were in agreement with independently determined values [32]. These four parameters strongly suggest that Marangoni convection was eliminated when thermal conduction through the funnel walls was eliminated, i.e., when water evaporated while maintained at the mouth of a PMMA funnel.

Marangoni convection was observed when H_2O and D_2O evaporated from the mouth of a stainless-steel funnel [13,14]. In those experiments, the throat was maintained at approximately the same temperature as in the experiments with the PMMA funnel. As a hypothesis and motivation for this study, we proposed that when the evaporation cooled the water at the interface below the temperature at the throat, thermal energy was conducted through the funnel walls to the periphery of the interface. Since the thermal conductivity of H_2O and D_2O is so much less than that of stainless steel, the temperature at the periphery of the interface was then greater than that of the liquid at the centerline of the funnel. The observed transition from a quiescent interface to a convecting interface took place when the temperature at the periphery of the interface was greater than that on the centerline. This *happened* to coincide with the Marangoni number being approximately 100 (Table III), and therefore seemed to have resulted from the instability mechanism discussed by Pearson [19]. But since the results obtained with the PMMA funnel do not indicate a transition from a quiescent to a convecting interface even when the Marangoni number is as high as 27 847, the convection observed in references [13,14] appears to have resulted from a temperature gradient along the interface.

One may then ask if the Pearson-Nield model is applicable when the liquid is volatile. The results of this study raise doubts. The Pearson-Nield model assumes the vapor could be treated as a *heat sink*, but as seen in Figs. 2 and 4 this is an invalid assumption: the vapor acts more as a *heat source* than a *heat sink*. It is not clear that interfacial energy transport during water evaporation can be correctly described using the empirical heat-transfer coefficient: the approach adopted in the Pearson-Nield model. As seen in Fig. 4 and Table III, there is an interfacial temperature discontinuity at the water-vapor interface in which the interfacial-vapor temperature is greater than that of the liquid. This observation is consistent with several earlier studies [13,16,30–35,40,41]. Pearson assumed the existence of a temperature discontinuity, but in the *opposite* direction of that observed.

However, the problems with the Pearson model disappear if the liquid is assumed to be nonvolatile. At present, there is not a method available that can be used to predict the conditions under which an evaporating liquid makes a transition from quiescent to a convecting interface. An approach is described in [42].

[1] R. D. Deegan, O. Bakajin, T. F. Dupont, G. Huber, S. R. Nagel, and T. A. Witten, Nature (London) **389**, 827 (1997).
[2] R. D. Deegan, Phys. Rev. E **61**, 475 (2000).
[3] R. D. Deegan, O. Bakajin, T. F. Dupont, G. Huber, S. R. Nagel, and T. A. Witten, Phys. Rev. E **62**, 756 (2000).
[4] W. D. Ristenpart, P. G. Kim, C. Domingues, J. Wan, and H. A. Stone, Phys. Rev. Lett. **99**, 234502 (2007).
[5] H. Hu and R. G. Larson, J. Phys. Chem. B **110**, 7090 (2006).
[6] H. Hu and R. G. Larson, Langmuir **21**, 3963 (2005).
[7] H. Hu and R. G. Larson, Langmuir **21**, 3972 (2005).
[8] S. Narayanan, J. Wang, and X.-M. Lin, Phys. Rev. Lett. **93**, 135503 (2004).
[9] D. J. Norris, E. G. Arlinghaus, L. Meng, R. Heiny, and L. E. Scriven, Adv. Mater. **16**, 1393 (2004).
[10] E. Rabani, D. R. Reichman, P. L. Geisser, and L. E. Brus, Nature (London) **426**, 271 (2003).
[11] M. Teitel, D. Schwabe, and A. Y. Gelfgat, J. Cryst. Growth **310**, 1343 (2008).
[12] C. A. Ward and F. Duan, Phys. Rev. E **69**, 056308 (2004).
[13] F. Duan and C. A. Ward, Phys. Rev. E **72**, 056302 (2005).
[14] F. Duan and C. A. Ward, Phys. Rev. E **72**, 056304 (2005).
[15] K. S. Das and C. A. Ward, Phys. Rev. E **75**, 065303(R) (2007).
[16] F. Duan, V. K. Badam, F. Durst, and C. A. Ward, Phys. Rev. E **72**, 056303 (2005).
[17] A. V. Hershey, Phys. Rev. **56**, 204 (1939).
[18] M. J. Block, Nature (London) **178**, 650 (1956).
[19] J. R. A. Pearson, J. Fluid Mech. **4**, 489 (1958).
[20] D. A. Nield, J. Fluid Mech. **19**, 341 (1964).
[21] E. L. Koschmieder and M. I. Biggerstaff, J. Fluid Mech. **167**, 49 (1986).
[22] M. F. Schatz, S. J. VanHook, W. D. McCormick, J. B. Swift, and H. L. Swinney, Phys. Rev. Lett. **75**, 1938 (1995).
[23] A.-T. Chai and N. Zhang, Exp. Heat Transfer **11**, 187 (1998).
[24] G. T. Barnes and A. I. Feher, J. Colloid Interface Sci. **75**, 584 (1980).
[25] H. K. Cammenga, D. Schreiber, and B.-E. Rudolph, J. Colloid Interface Sci. **92**, 181 (1983).
[26] H. K. Cammenga, D. Schreiber, G. T. Barnes, and D. S. Hunter, J. Colloid Interface Sci. **98**, 585 (1984).
[27] J. R. Taylor, *An Introduction to Error Analysis*, 2nd ed. (University Science Books, Sausalito, CA, 1982), p. 45.
[28] C. A. Ward, J. Chem. Phys. **79**, 5605 (1983).
[29] C. A. Ward, R. D. Findlay, and M. Rizk, J. Chem. Phys. **76**, 5599 (1982).

[30] C. A. Ward and G. Fang, Phys. Rev. E **59**, 429 (1999).
[31] C. A. Ward and D. Stanga, Phys. Rev. E **64**, 051509 (2001).
[32] F. Duan, I. Thompson, and C. A. Ward, J. Phys. Chem. B **112**, 8605 (2008).
[33] F. Duan, C. A. Ward, V. K. Badam, and F. Durst, Phys. Rev. E **78**, 041130 (2008).
[34] G. Fang and C. A. Ward, Phys. Rev. E **59**, 417 (1999).
[35] G. Fang and C. A. Ward, Phys. Rev. E **59**, 441 (1999).
[36] G. Herzberg, *Molecular Spectra and Molecular Structure* (Van Nostrand, Princeton, NJ, 1964), Vol. 2, p. 281.
[37] K. Feldkamp, Chem.-Ing.-Tech. **41**, 1181 (1969).
[38] G. S. Kell, J. Chem. Eng. Data **12**, 66 (1967).
[39] I. M. Thompson, M.A. thesis, University of Toronto, Toronto, Canada, 2007.
[40] V. K. Badam, V. Kumar, F. Durst, and K. Danov, Exp. Therm. Fluid Sci. **32**, 276 (2007).
[41] S. Popov, A. Melling, F. Durst, and C. A. Ward, Int. J. Heat Mass Transfer **48**, 2299 (2005).
[42] K. S. Das and C. A. Ward, Phys. Rev. E (to be published).